

Mechanisms of detachment in fibrillar adhesive systems

Pranav Sudersan^a, Michael Kappl^{a,*}

^a*Max Planck Institute for Polymer Research, Ackermannweg 10, 55128 Mainz, Germany*

Abstract

Several creatures can climb on smooth surfaces with the help of hairy adhesive pads on their legs. A rapid change from strong attachment to effortless detachment of the leg is enabled by the asymmetric geometry of the tarsal hairs. In this study, we propose mechanisms by which the hairy pad can be easily detached, even when the hairs possess no asymmetry. Here, we examine the possible function of the tibia-tarsus leg joint and the claws. Based on a spring-based model, we consider three modes of detachment: vertically pulling the pad while maintaining either a 1) fixed or a 2) free joint, or by 3) flexing the pad about the claw. We show that in all cases, the adhesion force can be significantly reduced due to elastic forces when the hairs deform non-uniformly across the array. Our proposed model illustrates the design advantage of such fibrillar adhesive systems, that not only provide strong adhesion, but also allow easy detachment, making them suitable as organs for fast locomotion and reliable hold. The presented approaches can be potentially used to switch the adhesion state in bio-inspired fibrillar adhesives, by incorporating artificial joints and claws into their design, without the need of asymmetric or stimuli-responsive fibrillar structures.

Keywords: fibrillar adhesion, reversible adhesion, contact splitting, beetle, biomechanics

*Corresponding author. *Telephone:* +49 6131 379-114
Email address: `kappl@mpip-mainz.mpg.de` (Michael Kappl)

1. Introduction

Over the past few decades, there have been numerous studies to understand how animals, such as geckos and insects, are able to walk on surfaces of any direction while seemingly defying gravity. A microscopic observation reveals that, in many cases, animals have a dense array of fibrillar structures at the end of their legs [1, 2]. These *hairy* adhesive pads help the animal to stay attached to any surface or detach easily at will for countless cycles, a property that is referred to as *reversible adhesion*. Previous attempts to theoretically explain adhesion in hairy pads [3, 4, 5] has followed two fundamental approaches: either by energy balance, or by force balance.

In the energy balance approach, adhesion is usually characterized by *work of adhesion* (W_{adh}), which is the energy required to separate a pad from the surface. During detachment, the elastic energy stored in the hair is dissipated, that increases W_{adh} and thus adhesion is enhanced [6, 7]. Detachment of an individual hair can be explained based on Kendall's peeling theory [8, 9], which predicts low adhesion at high peeling angles.

In the force balance approach, adhesion is characterized by *pull-off force*, F_p (or stress, σ_p), which is the minimum force necessary to separate two surfaces from contact. Based on a *cohesive zone model*, Hui et. al. [10] have identified two regimes of single hair detachment: 1) a *flaw sensitive* regime, where, for large hair radius, contact failure occurs due to crack propagation, initiated by a stress singularity at the edge of the hair, leading to low σ_p ; 2) a *flaw insensitive* regime, where, for small hair radius, the contact interface fails simultaneously, leading to high σ_p . Likewise, Tian et. al. [11] have shown that the spatula-shaped hair tips in a gecko's toe allows it to change adhesion by three orders of magnitude by laterally sliding and controlling the pulling angle to disorient the hairs. The detailed mechanics of the spatula-shaped hair design for controlling adhesion have been extensively studied by theoretical modelling [12, 13, 14, 15, 16, 17], artificial mimics [18, 19, 20, 21, 22] as well as in several biological systems [23, 24, 25]. Federle [26] has further argued that the curved shape of the hair

1 helps the pad to stay attached when pulled proximally and easily detached by
2 elastic recoil when pushed distally.

3 The theory presented so far suggests that a low detachment force of a fibrillar
4 adhesive pad can be achieved either by increasing the stress concentration by
5 peeling the pad at high angles, or by laterally shearing the pad before pull-off,
6 which requires the hairs to have an asymmetric geometry or curvature. However,
7 some insects like male dock beetles predominantly possess mushroom-shaped
8 hairs with flat discoid terminals on their pads [27], that are relatively less asym-
9 metric compared to the spatula-shaped hairs. These mushroom-shaped hairs
10 have in fact been shown to possess superior adhesion compared to the spatula-
11 shaped hairs [28, 18] and are generally resistant to detachment via lateral shear
12 [29]. Yet, how does the beetles possessing such mushroom-shaped hairs still
13 easily detach their legs during locomotion? Besides, from an application per-
14 spective, introducing asymmetry into the pillar geometry to construct spatula-
15 shaped artificial biomimetic adhesives for easy detachment is challenging due
16 to current limitations in fabrication techniques and difficulty in scaling-up [18].
17 Alternate strategies are thus desired to switch the adhesion state of symmet-
18 ric pillar arrays in a reversible manner. This can be achieved, for example, by
19 buckling the pillars under compressive load leading to their contact loss [30] or
20 by using special materials reacting to external stimuli such as magnetic field
21 [31], UV light [32] or temperature [33].

22 Employing the force-balance approach, in this work we theoretically model
23 the possible mechanisms by which adhesive pads with axially-symmetric hairs
24 can be easily detached, without the need of any spatula-like asymmetry. Here,
25 we focus our analysis on normal adhesion force necessary to separate the pad
26 from a flat surface under a purely mechanical action. We found that the max-
27 imum force necessary to detach the leg can be significantly reduced by strate-
28 gically controlling the tilt, joints and claws of the adhesive system. We hope
29 our work to provide new approaches to control the adhesion force of an artifi-
30 cial micro-pillar adhesive, that has applications in bio-inspired climbing robots,
31 pick-and-place operations and reusable adhesives.

1 2. Model

2 Similar to previous approaches [34, 35], the fibrillar adhesive pad is assumed
3 to be a one-dimensional array of N_t hairs, each behaving like a spring with spring
4 constant, k_h , and natural length, $l_{h,0}$ (Figure 1). The array backing is assumed
5 to be stiff. The pad is attached to a linearly deformable leg (tibia), assumed to
6 be another spring with spring constant, k_l , and natural length, $l_{l,0}$. The leg is
7 hinged to the array at a distance, s , from the right end of the array. The hinge,
8 analogous to the tibia-tarsus leg joint of an insect, is at a vertical distance, d_s ,
9 from the surface. The hairs are spaced apart by a width, w , and the array is of
10 length, $L = (N_t - 1)w$. The pad is oriented at an instantaneous angle, θ , while
11 making contact with a flat smooth surface. Each hair can attain a maximum
12 length, $l_{h,p}$, before pull-off, such that its pull-off force, $f_p = k_h (l_{h,p} - l_{h,0})$. F_{net}
13 is the net normal force on the pad and M_{net} is the the net moment about the
14 hinge, at a particular instant during the detachment process. We focus only
15 on vertical detachment modes and thus lateral friction forces between the hairs
16 and surface are not considered for our analysis.

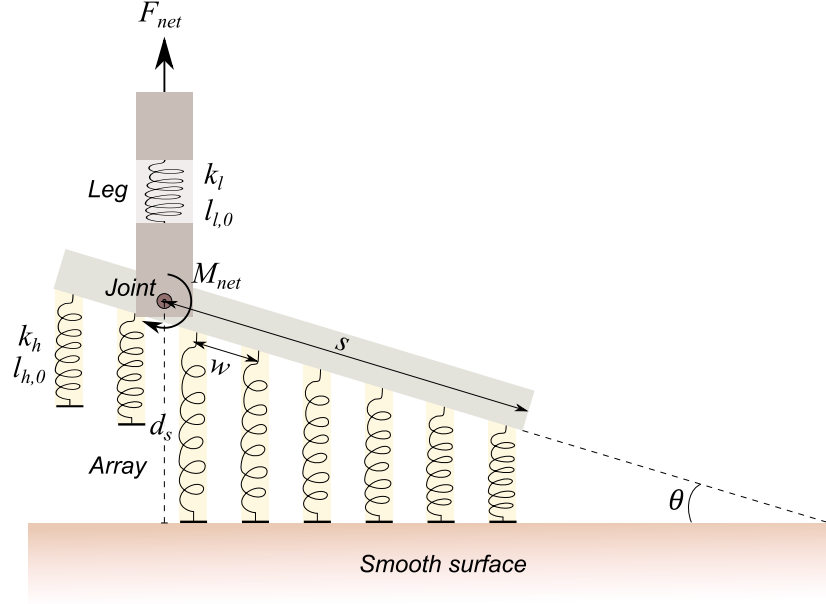


Figure 1: **Spring contact model of a fibrillar adhesive pad.** The pad consists of an array of N_t hairs connected to a deformable leg at the joint. At a particular distance, d_s , n number of hairs are in contact and the array is oriented at a tilt angle, θ , with the surface.

- 1 Suppose at a particular instant, there are n hairs in contact with the surface.
- 2 The net force on the whole pad will be,

$$F_{net} = \sum_{i=1}^n k_h (l_{h,i} - l_{h,0})$$

- 3 Simplifying, we get (see Appendix B for derivation):

$$F_{net} = nk_h [d_s - l_{h,0} - \Psi \sin \theta] \quad (1)$$

- 4 where, $\Psi = s - \frac{n-1}{2}w$. For a particular value of n , equation (1) is valid
- 5 until a certain distance, $d_{s,max}$, above which the left most hair will detach. Just
- 6 before detachment, this hair will be at its maximum length, $l_{h,p}$. From simple
- 7 geometry we can thus find:

$$d_{s,max} = l_{h,0} + \frac{f_p}{k_h} + [s - (n-1)w] \sin \theta \quad (2)$$

Equation (1) will be valid for $d_s \leq d_{s,max}$.

The maximum possible adhesion of the array would be the case when all hairs detach simultaneously ($\theta = 0^\circ$):

$$F_{max} = N_t f_p \quad (3)$$

The net moment, M_{net} , about the joint can be similarly derived (see Appendix B):

$$M_{net} = n k_h \cos \theta \left[(d_s - l_{h,0}) \Psi - \left\{ \Psi^2 + \frac{n^2 - 1}{12} w^2 \right\} \sin \theta \right] \quad (4)$$

Let us now consider the scenario where even the leg above the joint can undergo elastic stretching together with the hairs. When a hair detaches from the surface, the leg undergoes an elastic recoil due to the stored elastic energy. Suppose the leg relaxes upward by a recoil length, Δl , at the point of the joint. For n hairs in contact, ~~the~~ when a hair detaches, the array's tilt angle will change from initial θ_b to θ_a as a result of joint rotation. The i^{th} hair of the array thus deforms by Δl_i , which by geometry, is derived as:

$$\Delta l_i = \Delta l + i w (\tan \theta_a - \tan \theta_b) \quad (5)$$

The force balance before and after a hair detaches is thus given respectively by:

$$\begin{aligned} \sum_{i=1}^n k_h (l_{h,i} - l_{h,0}) &= k_l (l_l - l_{l,0}) \\ \sum_{i=1}^{n-1} k_h (l_{h,i} + \Delta l_i - l_{h,0}) &= k_l (l_l - \Delta l - l_{l,0}) \end{aligned}$$

Solving the above two equations with equation 5 for Δl , we get:

$$\Delta l = \frac{f_p}{k_h (n-1) + k_l} \frac{f_p - k_h w (n/2) (n-1) (\tan \theta_a - \tan \theta_b)}{k_h (n-1) + k_l} \quad (6)$$

Thus, d_s shifts by Δl in equations 1 and 4 at each event of hair detachment (i.e. when $d_s = d_{s,max}$).

We express the forces and distances in non-dimensional forms, as below:

$$\hat{f}_p = \frac{f_p}{k_h w}, \quad \hat{F}_{net} = \frac{F_{net}}{k_h w}, \quad \hat{d}_s = \frac{d_s - l_{h,0}}{w}, \quad \hat{s} = \frac{s}{L}$$

Here, \hat{f}_p is a parameter which encapsulates the hair's adhesion force, stiffness and array density. Unless specified, positive force values represent attraction by convention. [Python scripts were written to solve the above equations under specific detachment conditions \(available in the public repository https://github.com/PranavSudersan/paper-effect_of_tilt/blob/main/codes/Fibrillar%20adhesion%20-%20Effect%20of%20tilt.ipynb\)](https://github.com/PranavSudersan/paper-effect_of_tilt/blob/main/codes/Fibrillar%20adhesion%20-%20Effect%20of%20tilt.ipynb)

3. Detachment mechanisms

We consider three tentative scenarios to detach the adhesive pad from a surface: 1) *Fixed pull*, where the pad is pulled vertically up while keeping a fixed joint; 2) *Free pull*, where the pad is pulled vertically up while keeping the joint free to allow rotation of the array; 3) *Flex*, where the pad is hinged to an external point (claw-hinge), and detached in a rotary fashion, emulating the claw function in insects. To investigate each case in detail, let us assume a pad to be a one-dimensional analogue of a dock beetle's adhesive pad [27, 36] with $N_t = 25$ hairs and $\hat{f}_p = 0.1$ (see discussion on *detachment pathways* for details) attached to a stiff leg (or tibia) with $k_l \rightarrow \infty$. The situation of a soft leg with $k_l/k_h = 10$ is also considered for the first two cases involving vertical detachment.

3.1. Fixed pull

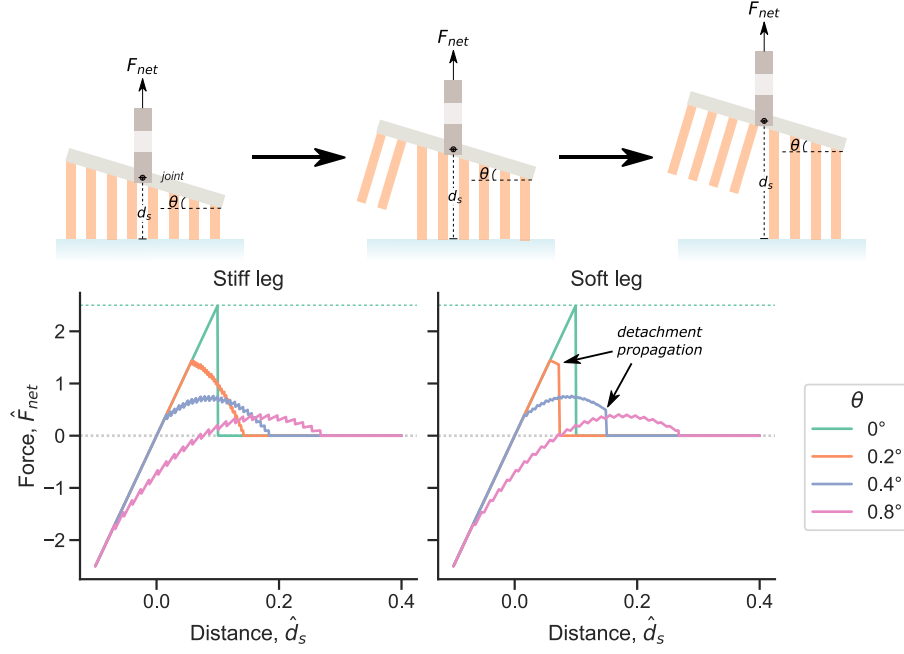


Figure 2: **Detachment by Fixed Pull.** Force-distance curves for a fibrillar adhesive pad, pulled vertically upwards with a fixed joint. The tilt angle, θ , of the array is kept fixed during detachment. The leg (tibia) is either stiff ($k_l \rightarrow \infty$) or soft ($k_l/k_h = 10$). Positive force values represent attraction between the array and the surface. The green dashed line represents the maximum possible adhesion for the pad. All values are normalized to dimensionless forms, as described in text.

The fibrillar adhesive pad can be detached by pulling it vertically upwards while maintaining a constant tilt angle, θ , with the surface. This can be achieved if the joint is kept fixed. Equations 1, 2 and 3 can be used to get the resulting force-distance curves for such a scenario. To summarize the numerical procedure in brief, we start with an initial $n = 25$ hairs. F_{net} is then calculated for increasing d_s , until $d_s = d_{s,max}$, upon which n value is decremented by 1. The above process is repeated for increasing d_s until $n = 0$, indicating complete detachment. For the case of the soft leg, on each instance when n is decremented, d_s is increased by an additional Δl value (equation 6) in order to account for

1 the recoil effect of the leg.

2 Increasing the tilt of the pad decreases its maximum force or adhesion (Fig-
3 ure 2). Tilting the pad causes an inhomogeneous deformation of hairs, where,
4 on one end they are stretched, while, on the other end they are compressed.
5 The balance of the respective attractive and repulsive elastic forces of the hairs
6 ultimately results in a decrease in the net force. The tilted orientation also
7 causes the individual hairs to detach distinctly rather than simultaneously, fur-
8 ther reducing the maximum adhesion of the array. We term this effect of loss
9 in adhesion due to a non-uniform hair deformation across the array as *elastic*
10 *weakening*. When there is no tilt ($\theta = 0^\circ$), all the hairs undergo identical defor-
11 mation and ultimately detach simultaneously after a distance, $\hat{d}_s = 0.1$. Here,
12 no *elastic weakening* occurs and the pad shows the maximum possible adhesion.

13 For the case of a stiff leg (tibia), we see that at small distances, all hairs
14 of the pad are in contact with the surface, resulting in a linear force response.
15 On further pulling, the hairs will start to detach sequentially from left to right,
16 indicated by a characteristic saw-tooth jitter in the force curves. The ~~hairs of~~
17 ~~the pad with a higher tilt angle will start to detach first, followed by the ones~~
18 initiates hair detachment first, in comparison to a pad with a lower tilt.

19 For the case of a soft leg (tibia), we observe a similar effect of tilt angle
20 on the force curves as before. The maximum adhesion force at a particular
21 tilt is the same as that for the stiff leg. The saw-tooth jitter are however
22 minimized due to the leg's deformation, leading to a dampened force response.
23 Interestingly, the force abruptly drops to zero for the angles 0.2° and 0.4° . This
24 is an effect of the elastic recoil of the leg while each hair loses contact during the
25 detachment process (equation (6)). The length difference between the detached
26 hair just before it breaks contact and its adjacent hair is $w \sin \theta$. If the leg's
27 recoil length, $\Delta l > w \sin \theta$, the adjacent hair will be stretched more than its
28 maximum length ($l_{h,p}$), and thus will also detach, leading to further recoil of
29 the leg. Equation (6) shows that Δl increases with every subsequent loss of
30 hair contact if θ is kept constant ~~—(i.e. $\theta_b = \theta_a$).~~ This implies that, once
31 initiated, the leg's recoil will always be large enough to detach every remaining

1 hair, resulting in a spontaneous propagation of the detachment front until the
 2 pad completely breaks contact with the surface. This is consistent with a recent
 3 report of catastrophic failure, due to a similar recoil effect of the measurement
 4 system, seen in micro-fibrillar adhesives with a narrow variance of individual
 5 fibril adhesive strengths [37].

6 3.2. Free pull

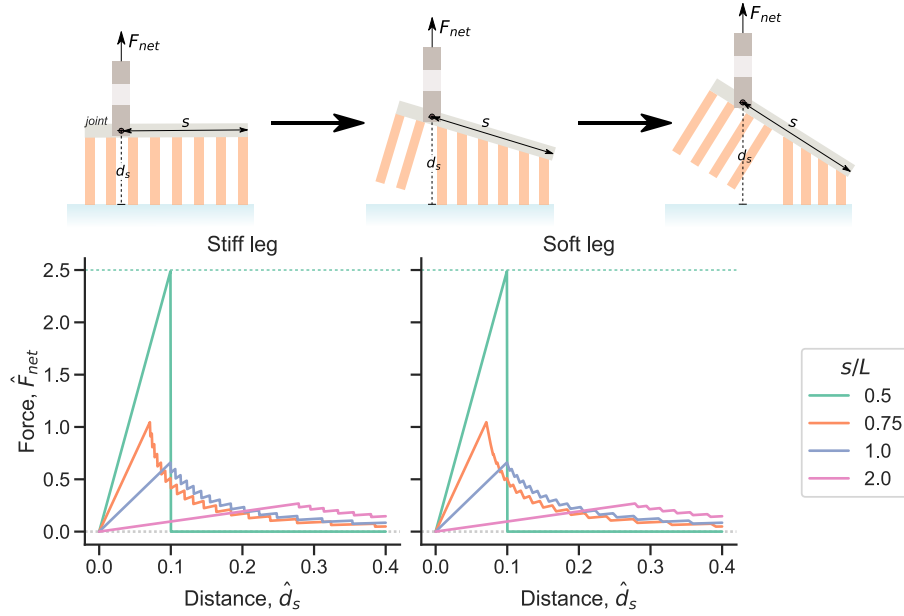


Figure 3: **Detachment by Free Pull.** Force-distance curves for a fibrillar adhesive pad, pulled vertically upwards with a free joint. s is the distance between the joint and the right end of the array and L is the array length. The free joint allows further tilting of the array during the vertical pull. The leg (tibia) is either stiff ($k_l \rightarrow \infty$) or soft ($k_l/k_h = 10$). Positive force values represent attraction. The green dashed line represents the maximum possible adhesion for the pad. All values are normalized to dimensionless forms, as described in text.

7 Similar to the previous case, we once again consider the situation where the
 8 adhesive pad is pulled vertically upwards for detachment. However now, the
 9 joint is assumed to be freely movable. In this case, the array will reorient itself
 10 to maintain a zero net moment about the joint during the entire detachment

1 process. At any given instant, the tilt angle, θ , can be found by setting M_{net} to
 2 zero in equation (4) to get:

$$\theta(\hat{d}_s, n) = \arcsin \left[\frac{(\hat{s} - \frac{n-1}{2}) \hat{d}_s}{(\hat{s} - \frac{n-1}{2})^2 + \frac{n^2-1}{12}} \right] \quad (7)$$

3 Using the above relation together with equations 1, 2 and 3, we can find
 4 force-distance curves during a free vertical pull of the adhesive pad. [A similar](#)
 5 [numerical procedure as *fixed pull* is followed here.](#) Since the position of the joint
 6 will influence the net moment, we use the ratio, s/L , to study its effect on the
 7 detachment forces.

8 Maximum adhesion is seen when the joint is positioned at the centre of the
 9 array, i.e. $s/L = 0.5$ (Figure 3). Here, the net moment due to the hairs is
 10 balanced by symmetry and the array remains parallel to the substrate until
 11 all hairs detach simultaneously at $\hat{d}_s = 0.1$. Shifting the position of the joint
 12 further away from the array centre leads to lower forces or adhesion. The re-
 13 sulting moment imbalance will tilt the array, which reduces the net force due to
 14 the *elastic weakening* effect, as described in the previous section. Higher s/L
 15 increases the net moment to be balanced, leading to a higher tilt of the array
 16 and thus lower net force.

17 The force curves look qualitatively different compared to the previous case of
 18 *fixed pull*. A sharp maxima is seen, coinciding with the point when the first hair
 19 detaches. Beyond this, the force starts to decrease sharply and once again shows
 20 the characteristic saw-tooth jitter as the subsequent hairs detach in sequence.
 21 Nearly identical trend is seen for both a stiff and a soft leg (tibia). The elastic
 22 recoil of the leg does slightly reduce the amplitude of the jitter for the soft leg
 23 case. However, no abrupt drop in the force is seen like before. As the hairs
 24 detach, the array gets tilted more and more (i.e. $\theta_b < \theta_a$), making it less likely
 25 for the recoil length, Δl , to exceed $w \sin \theta - w \sin \theta_a$ and detach the next adjacent
 26 hair. Thus here, we don't see any propagation of the detachment front when
 27 the leg is soft.

3.3. Flex

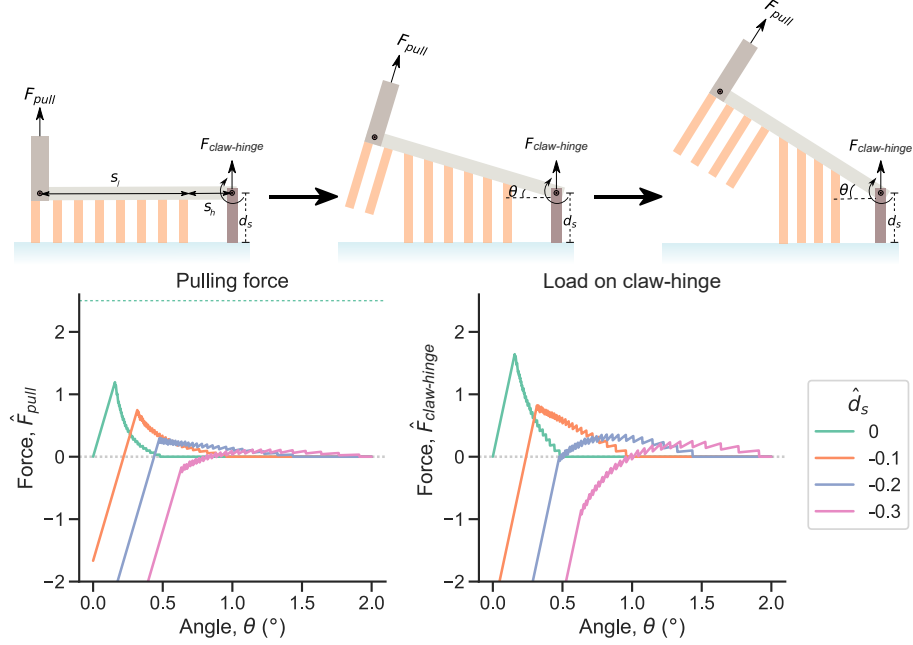


Figure 4: **Detachment by Flex.** Force curves for a fibrillar adhesive pad detached by flexing it about the claw. $\hat{F}_{pull} = \frac{F_{pull}}{k_h w}$ is the normalised pulling force necessary to apply the moment about the claw-hinge for detachment, $\hat{F}_{hinge} = \frac{F_{hinge}}{k_h w}$ is the normalised reaction force on the claw-hinge, $\hat{d}_s = \frac{d_s - l_{h,0}}{w}$ is the normalized vertical distance of the claw-hinge from the surface. Here, $s_l/L = 1$ and $s_h/w = 10$. The green dashed line represents the maximum possible adhesion for the pad.

Instead of a vertical pull, the adhesive pad can also be detached by rotating it about the claw-hinge, located outside the array. Such a mode of detachment will be driven by a moment applied by the leg (tibia) to rotate the pad around the claw-hinge until all the hairs lose contact. Let s_h be the distance between the claw-hinge and the right end of the array; s_l be the distance between the joint and the right end of the array. The joint is assumed to be fixed here. To illustrate the mechanism, let us fix $s_l/L = 1$ (here, $L = 24w$) and $s_h/w = 10$ and vary the vertical claw-hinge distance, d_s . At any particular instant, the pulling force applied by the leg, $F_{pull} = M_{net}/(s_l + s_h)$, where M_{net} is obtained by

1 setting $s = -s_h$ in equation (4). Equation (1) will give us the reaction force
 2 acting on the claw-hinge, $F_{claw-hinge}$.

3 Decreasing the vertical claw-hinge distance reduces the pulling force nec-
 4 essary to undergo detachment by flexing (Figure 4). One can imagine that
 5 initially, when the array is parallel to the surface, a lower value of d_s means the
 6 hairs are in a more compressed state. When the pad is subsequently rotated
 7 around the claw-hinge, the tilted array will once again lead to an *elastic weak-*
 8 *ening* effect due to the inhomogeneous deformation of hairs. This results in a
 9 decrease in the net moment and thus lower F_{pull} for smaller values of d_s . F_{pull}
 10 can be further reduced of course by increasing the lever arm ($s_l + s_h$).

11 Detachment by flexing requires that the claw remains fixed and stable dur-
 12 ing the process. We see that generally, the normal load, acting on the hinge,
 13 $F_{claw-hinge}$, follows a similar trend as F_{pull} (Figure 4). For low values of d_s ,
 14 $F_{claw-hinge}$ goes to negative values, implying that the claw should ~~adhere~~ stick
 15 well with the surface, perhaps by mechanical interlocking, to resist this negative
 16 load. As the detachment progresses however, the array starts to exert a positive
 17 load on the claw.

18 4. Discussion

19 In order to characterize how a particular detachment mechanism influences
 20 the adhesion of the pad, we introduce a parameter, *reduction factor*, defined as:

$$r = \frac{N_t f_p}{F_{adh}} \quad (8)$$

21 Here, F_{adh} is the adhesion force required to detach the pad from the surface
 22 following a given mechanism and $N_t f_p$ is the maximum possible adhesion of
 23 the pad (equation (3)). Reduction factor, r , represents the extent to which the
 24 adhesion can be reduced by choosing the mode of detachment. A large value
 25 of r implies that adhesion can be reduced by a greater factor, and this mode is
 26 more suitable to easily detach.

1 *Effect of \hat{f}_p :* The dimensionless parameter, $\hat{f}_p = \frac{f_p}{k_h w}$, governs the strength and
2 compliance of the array, where, high values represent a dense array of strongly
3 adhering soft hairs. Let us consider the case of an adhesive pad with $N_t = 25$
4 hairs and look at how \hat{f}_p influences the reduction factor under each mode of
5 detachment (Figure 5).

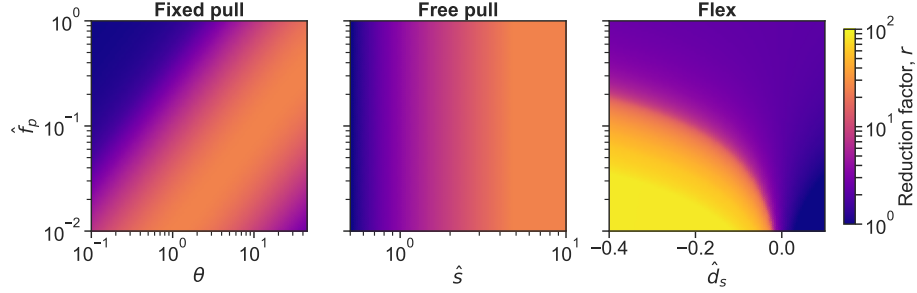


Figure 5: **Effect of \hat{f}_p on reduction factor.** Colour plots showing the effect of the dimensionless parameter, \hat{f}_p , on the reduction factor for each mode of detachment. Here, we fix the number of hairs, $N_t = 25$. The dimensionless parameters $\hat{d}_s = \frac{d_s - l_{h,0}}{w}$ and $\hat{s} = \frac{s}{L}$, as described in text.

6 When detachment follows the *fixed pull* method (Figure 5), for a constant \hat{f}_p ,
7 the reduction factor increases with increasing tilt angle, θ , and then decreases,
8 showing a maximum r of 25 at an intermediate θ . Higher values of \hat{f}_p shifts this
9 maximum point to higher values of θ . This trend relates to the *elastic weakening*
10 effect discussed before. Smaller values of θ bring a proportion of hairs under
11 compression, reducing the adhesion and thus increasing r . On further tilting
12 the array, eventually the proportion of stretched hairs will overcome the ones
13 under compression, which ultimately reduces r at high θ . When the individual
14 hairs show strong adhesion (i.e. for high \hat{f}_p), a greater tilt is necessary to bring
15 the net adhesion of the array down.

16 For the case of detachment via *free pull*, \hat{f}_p has no influence on the reduction
17 factor. On the other hand, shifting the position of the joint further away from
18 the array (i.e. high s/L) results in large values of r . In this scenario, the
19 higher moment exerted by the array leads to a higher tilt, and thus increases

1 the reduction factor via *elastic weakening*, saturating to the maximum value of
2 25.

3 For detachment by *flexing*, the reduction factor increases for higher initial
4 compression of hairs (low \hat{d}_s). The pad notably shows a much higher reduction
5 factor at low values of \hat{f}_p and \hat{d}_s , with values as high as 100. Since this mode
6 of detachment is driven by moment, the pulling force necessary to provide the
7 moment can be decreased without any limit simply by having a long lever arm
8 (\hat{s}_l), i.e., with the joint positioned farther away from the array. In contrast, for
9 the previous cases of *free pull* and *fixed pull*, the reduction factor is capped to
10 the maximum number of hairs in the array ($N_t = 25$). Here, *elastic weakening*
11 can only reduce the array's adhesion force from N_t hairs down to a single hair
12 at most.

13 *Effect of N_t :* Let us now fix $\hat{f}_p = 0.1$ and investigate the influence of the number
14 of hairs, N_t , on the reduction factor (Figure 6). The colour plots show that high
15 N_t increases r irrespective of the mode of detachment. Under a tilted state, more
16 hairs are compressed when N_t is high, which reduces the net adhesion. This
17 highlights ~~the~~another advantage of having a split contact design found in many
18 biological systems. A ~~higher~~design comprising of a large number of hairs ~~offers~~
19 not only enhances the adhesion due to scaling effects [38], but could also offer a
20 better control over adhesion~~and thus is more suited~~, making it quite suitable for
21 reversible attachment and detachment during locomotion. The specific trends
22 of reduction factor for each mode of detachment can be understood by similar
23 arguments of *elastic weakening*, as discussed in the previous section.

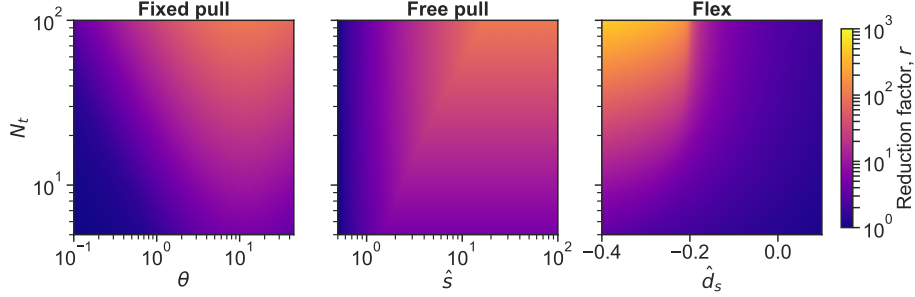


Figure 6: **Effect of N_t on reduction factor.** Colour plots showing the effect of the number of hairs, N_t , on the reduction factor for each mode of detachment. Here, we fix the dimensionless parameter, $\hat{f}_p = 0.1$. The dimensionless parameters $\hat{d}_s = \frac{d_s - l_{h,0}}{w}$ and $\hat{s} = \frac{s}{L}$, as described in text.

Figures 5 and 6 can be combined into a single set of colour plots by defining a new dimensionless parameter, $\chi = \hat{f}_p N_t = \frac{f_p N_t}{k_h w}$ (see Appendix A). Overall, we see that *flex* mode of detachment shows the highest reduction factor among the three modes, with the optimal value of $\chi \sim 1$.

Detachment pathways: Based on the three modes of detachment discussed in the previous sections, one can think of several strategies to detach fibrillar adhesive pads from the surface. To illustrate this, let us consider the adhesive system of a dock beetle. The beetle is known to have 3 sets of hairy tarsal adhesive pads in each of their legs, each possessing hairs of different geometries. To keep our analysis simple, we will assume each leg to have only two adhesive pads, with identical hairs of mushroom-shaped geometry. The distal and proximal pads possess roughly 500 and 1000 hairs, respectively [27]. Assuming the pads to be rectangular arrays of 20×25 and 40×25 hairs, we can model this as a one-dimensional system of 20 and 40 *effective hairs*, respectively, by combining the hairs along the width. Based on reported measurements [36], the beetle's *effective hair* is thus considered to have an effective pull-off force, $f_p = 0.5 \times 25 = 12.5 \mu\text{N}$ and effective spring constant, $k_h = 0.5 \times 25 = 12.5 \text{ N m}^{-1}$. The beetle's hairs are approximately $l_{h,0} = 40 \mu\text{m}$ long, spaced $w = 10 \mu\text{m}$ apart. At end of the tarsal segments, there is a claw, around $200 \mu\text{m}$ long, and

1 the leg (tibia) is connected roughly at the end of the proximal tarsal pad. This
2 will put $\hat{s}_h = 20$ and $s_l/L = 1$, measured relative to the right end of the distal
3 pad. The beetle's leg is assumed to possess two joints which could serve as a
4 hinge for rotation during detachment (H_1 and H_2 in Figure 7 inset). The claw
5 can be used as an external hinge (H_3) by flexing the tarsal pad around it.

6 Based on the above assumptions, we can come up with force-distance curves
7 to detach the beetle's leg via various pathways (Figure 7). First, let us assume
8 the joint H_2 to be fixed, such that both the distal and proximal pads can be
9 combined to behave like a single long pad with $N_t = 60$ hairs. Path 1 shows
10 the case where the pad shows maximum possible adhesion. Here, the combined
11 pad is vertically pulled upwards while keeping the array perfectly parallel to the
12 surface. If this combined pad is detached by keeping H_1 fixed and maintaining
13 a tilt of 1° with the surface (path 2), the forces dramatically reduces, with
14 around 10 times reduction in the adhesion compared to path 1. We can also
15 detach the pad by switching between the different mechanisms. Path 3 shows
16 one such example, where, initially the leg is pulled vertically up while keeping
17 H_1 fixed, stretching the hairs similar to path 1. On reaching point a , H_1 is set
18 free, which results in a sudden drop in force due to the excess moment by the
19 stretched hairs, tilting the array. Beyond this, the force curve follows the *free*
20 *pull* mechanism, with ~ 3.5 times reduction in adhesion. An alternate strategy
21 of switching between mechanisms would be to first apply a load on the pad (path
22 4) and compress the hairs until point b . Beyond this point, the claw can be used
23 as a hinge to detach the pad via flexing it around H_3 , which once again reduces
24 the adhesion force. Now, if we assume the joint H_2 to be free such that the two
25 pads can behave distinctly, we can consider the scenario where the proximal pad
26 is flexed around the distal pad at H_2 while keeping H_1 fixed (path 5). After the
27 proximal pad has completely detached, H_1 can be freed up at point c to detach
28 the distal pad via *free pull* with very little force. This pathway results in a ~ 5
29 times reduction in adhesion.

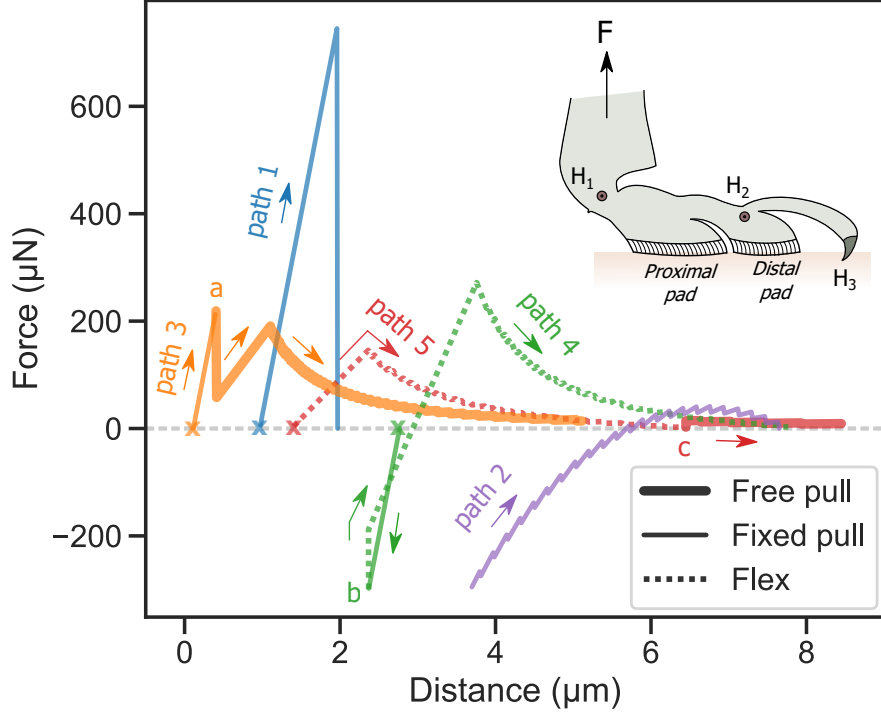


Figure 7: **Beetle leg detachment pathways.** Force curves showing the theoretical detachment pathways possible for a dock beetle's leg, as function of distance between the pad and the surface. The curves are offset laterally for clarity. Colours represent the distinct detachment pathways, labelled as path 1 to 5, with arrows indicating the direction of retraction. Points a, b and c indicate instances of switching between the different detachment mechanisms for paths 3, 4 and 5 respectively (see text for details). The different line style denotes the specific detachment mechanism followed by any region of the pathway. The inset schematic shows the assumed locations of the different joints or hinges (H_1 , H_2 and H_3) employed by the leg.

1 The above analysis illustrates how the design of the beetle's hairy adhesive
2 pads is suitable for modulating its adhesion. Effective control and release of its
3 joints can help the insect to reduce the pad's adhesion, allowing it to detach
4 with little effort. High reduction in adhesion is seen when the pad is tilted
5 relative to the surface during detachment, as a result of *elastic weakening*. To
6 the best of our knowledge, there is no direct experimental evidence that beetles
7 or any other animal can modulate its adhesion by taking advantage of this

1 effect. Considering that hair deformation occurs at length scales below 10 μm ,
 2 direct observation of this effect on running beetles would be challenging. A
 3 recent study on PDMS micro-pillar arrays, however, does indeed show a strong
 4 reduction in the adhesion force due to slight misalignments with the surface
 5 [39]. Based on previously reported microscopic investigation of freely walking
 6 dock beetles [40], we argue that the following experimental observations provide
 7 support to our proposed model: 1) The detachment was shown to follow a
 8 three-dimensional twist of the leg, which suggests a complex inhomogeneous
 9 deformation of hairs across the array, leading to *elastic weakening*, which is
 10 suited for easy detachment. Similar twisting action during detachment was
 11 also observed in flies [41] and has been used to easily detach mushroom-shaped
 12 artificial adhesive arrays [42]. 2) The beetle can at times instantaneously detach
 13 all its legs and drop itself while upside down. This could be explained by the
 14 beetle freeing up its joints and using just its body weight to provide the necessary
 15 force to detach all its legs via *free pull* (similar to path 3 above). [Lateral video](#)
 16 [recordings showed that in this scenario, claws were the last to detach when a leg](#)
 17 [loses contact with the surface, which also indicates a *flex* mode of detachment](#)
 18 [\(similar to path 5\).](#) 3) Only a fraction of the beetle's pads made contact with
 19 the surface during locomotion, which indicates that the pads should naturally
 20 be in a slightly tilted state. This not only reduces the contact area, but also non-
 21 uniformly deforms the hairs, both leading to a reduction in adhesion for easy
 22 detachment. 4) Contact images showed that the array *peels* from the proximal
 23 to distal direction during detachment. However, the beetle's hairs are attached
 24 to a relatively stiff backing [43], so it wouldn't be able to *peel* its array, since
 25 peeling, strictly speaking, depends on the elastic contribution of a thin flexible
 26 backing as it bends during the process [8]. Rather, the *peeling* observed in the
 27 beetle's case should be a result of the pad detaching from the surface in a tilted
 28 orientation, causing the hairs to distinctly detach in sequence. 5) The time
 29 scale of detachment was reported to be an order of magnitude shorter than the
 30 attachment time scale, which could be a result of the elastic recoil of the leg
 31 causing a spontaneous propagation of the detachment front (Figure 2).

1 There exists a limit to how much the pad can tilt, depending on its geometry
2 and material properties. Suppose the hair has a maximum linear elastic strain
3 limit, ε_m , and natural length, $l_{h,0}$. Based on Figure 1, if the right most hair is
4 compressed to its elastic limit, one can derive from simple geometry, that, the
5 corresponding maximum limit in tilt angle is given by:

$$\theta_{limit} = \arctan \frac{l_{h,0}\varepsilon_m}{(N_t - 1)w}$$

6 θ_{limit} will limit the reduction factor for each of the detachment mechanisms
7 presented. Longer hairs can result in a lateral collapse or bundling of hairs,
8 imposing an additional constraint on θ_{limit} . Large deformation of hairs can
9 also lead to buckling, which will further limit the reduction in adhesion due to
10 the smaller effective modulus. Buckling could also, interestingly, promote easier
11 detachment in the *free pull* mode. When the compressed hairs at one end of the
12 array buckle, there would be an excess clockwise moment in the array system
13 (Figure 3). This excess moment could subsequently drive the detachment of the
14 remaining hairs. In the case of biological systems, the ability of an insect to
15 provide the load necessary to tilt and compress its hairy adhesive pad against
16 the surface would further introduce limitations to follow any of the detachment
17 modes discussed here. All things considered, the geometry and elastic properties
18 of the individual hairs are crucial parameters to consider in the design of an
19 optimal array system which shows reversible adhesion via *elastic weakening*.

20 Our analysis had been limited to normal forces during detachment. A similar
21 analysis considering the energy required to detach the array will however not
22 yield any *elastic weakening* effect. Since we had assumed a purely elastic system,
23 the initial and final energy of the system would be the same regardless of the
24 mode of detachment, and thus the work of adhesion would remain identical in
25 all scenarios. The reduction of adhesion force is however advantageous since an
26 insect wouldn't then need a strong muscular to system to detach its legs, which
27 are typically capable of attachment forces several times its body weight [44].

28 5. Conclusion

~~Inhomogeneous deformation of hairs results in significant reductions in the~~
~~adhesion of~~ Controlled detachment of a fibrillar system similar to an insect's
tarsal hairy adhesive pads ~~Such a condition~~ can be achieved by either 1) pulling
the pad while maintaining a constant tilt angle, 2) pulling the pad while main-
taining a free tibia-tarsus leg joint or 3) flexing the pad around the claw. In all
three scenarios, an inhomogeneous deformation of hairs across the array results
in significant reductions in the net adhesion due to an elastic effect. Strategic
control of the joint's mobility or claw can allow the leg to easily switch between
the above mechanisms, thus providing a simple way to reduce adhesion as per
necessity. The presence of a deformable leg can further trigger a spontaneous
propagation of hair detachment due to the leg's elastic recoil, making it suitable
for fast detachment. Arrays with low \hat{f}_p and large number of hairs, with a hair
geometry that allows for large deformations while avoiding buckling and lateral
bundling represent the optimal design conditions to maximize the range of con-
trol over adhesion. The proposed model ~~is supported by~~ has been compared
with previously reported experimental observations of leg detachment in dock
beetles and highlights possible role of the joint and claws to enable reversible
adhesion. Similar strategies could potentially be adopted in the design of bio-
inspired artificial fibrillar adhesives to easily switch the adhesion state without
the need of asymmetric structures.

6. Acknowledgment

We are grateful to Prof. Dr. Hans-Jürgen Butt and Dr. Thomas Endlein
(Max Planck Institute for Polymer Research, Germany) for reviewing the text,
and thank Dr. Renè Hensel (Leibniz Institute for New Materials, Germany)
and Dr. Bat-El Pinchasik (Tel-Aviv University, Israel) for fruitful discussions.
This work was supported by the Deutsche Forschungsgemeinschaft [Grant num-
ber: PI 1351/2-1] and the Max Planck Graduate Center with the Johannes
Gutenberg-Universität Mainz [MPGC].

1 Appendix A. Reduction factor: master plot

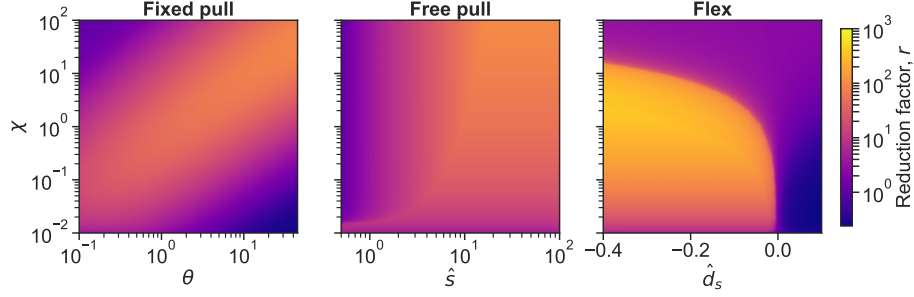


Figure A.1: **Effect of χ on reduction factor.** Here, we define a unified dimensionless design parameter $\chi = \frac{\hat{f}_p N_t}{k_h w}$, combining \hat{f}_p and N_t into a single number. The dimensionless parameters $\hat{d}_s = \frac{d_s - l_{h,0}}{w}$ and $\hat{s} = \frac{s}{L}$, as described in text.

2 Appendix B. Derivations

Suppose at a particular instant (Figure 1), there are n hairs in contact with the surface. The centre of the region of the array in contact is at a vertical distance, d' , from the surface. The net force on the whole array is,

$$F_{net} = \sum_{i=1}^n k_h (l_{h,i} - l_{h,0})$$

$l_{h,i}$ is the length of the i^{th} hair, which is at a horizontal distance, x_i , from the centre of the contact region. By simple geometry, $l_{h,i} = d' - x_i \tan \theta$. Substituting $l_{h,i}$ in above and noting that $\sum_{i=1}^n x_i = 0$ by symmetry, we get:

$$F_{net} = nk_h (d' - l_{h,0})$$

From geometry, d_s and d' is related as:

$$\frac{d_s}{\sin \theta} - \frac{d'}{\sin \theta} = s - \frac{(n-1)w}{2}$$

Substituting for d' , the net force, F_{net} , on the pad as a function of distance, d_s , is:

$$F_{net} = nk_h \left[d_s - l_{h,0} - \left[s - \frac{(n-1)w}{2} \right] \sin \theta \right]$$

1 The above equation is valid for $d_s \leq d_{s,max}$ at a particular value of n . We
2 can get $d_{s,max}$ by considering the situation just before the left most hair is about
3 to detach (Figure 1). This hair will be at its maximum length, $l_{h,p}$. Once again
4 from geometry, we see that $d_{s,max}$ and $l_{h,p}$ is related as:

$$\frac{l_{h,p}}{\sin \theta} - \frac{d_{s,max}}{\sin \theta} = (n-1)w - s$$

5 Substituting $l_{h,p} = \frac{f_p}{k_h} + l_{h,0}$ in above and simplifying, we get:

$$d_{s,max} = l_{h,0} + \frac{f_p}{k_h} + [s - (n-1)w] \sin \theta$$

6 The net moment about the joint due to the deformed hairs of the array is,

$$M_{net} = \sum_{i=1}^n \lambda_i k_h (l_{h,i} - l_{h,0}) \cos \theta$$

7 Here, $\lambda_i = s - \left(\frac{n-1}{2}w - \frac{x_i}{\cos \theta}\right)$ is the length of the lever arm between the i^{th}
8 hair and the joint.

9 Substituting for $l_{h,i}$ and eliminating d' as before, we get:

$$M_{net} = \sum_{i=1}^n k_h \cos \theta \left[s - \left(\frac{n-1}{2}w - \frac{x_i}{\cos \theta} \right) \right] \left[d_s - \left(s - \frac{(n-1)w}{2} \right) \sin \theta - x_i \tan \theta - l_{h,0} \right]$$

10 To calculate $\sum_{i=1}^n x_i^2$, we follow:

$$\sum_{i=1}^n x_i^2 = 2 \sum_{i=1}^{\frac{n}{2}} x_i^2 = 2 \sum_{i=1}^{\frac{n}{2}} \left[w \cos \theta \left(i - \frac{1}{2} \right)^2 \right] = 2w^2 \cos^2 \theta \left[\sum_{i=1}^{\frac{n}{2}} i^2 - \sum_{i=1}^{\frac{n}{2}} i - \sum_{i=1}^{\frac{n}{2}} \frac{1}{4} \right]$$

11 Using the identities $\sum_{i=1}^N i^2 = \frac{N(N+1)}{2}$ and $\sum_{i=1}^N i = \frac{N(N+1)}{2}$ and simpli-
12 fying, we get $\sum_{i=1}^n x_i^2 = n \left(\frac{n^2-1}{12} \right) w^2 \cos^2 \theta$. This, together with $\sum_{i=1}^n x_i = 0$ (by
13 symmetry), the expression for M_{net} above can be simplified to finally get:

$$M_{net} = nk_h \cos \theta \left[(d_s - l_{h,0}) \left[s - \frac{(n-1)w}{2} \right] - \left\{ \left[s - \frac{(n-1)w}{2} \right]^2 + \frac{n^2-1}{12} w^2 \right\} \sin \theta \right]$$

1 **References**

- 2 [1] R. Hooke, Micrographia, or, Some physiological descriptions of minute bod-
3 ies made by magnifying glasses : with observations and inquiries thereupon,
4 The Royal Society, London, 1665.
- 5 [2] N. E. Stork, Experimental analysis of adhesion of *Chrysolina Polita*
6 (chrysomelidae: Coleoptera) on a variety of surfaces, J Exp Biol 88 (1)
7 (1980) 91.
- 8 [3] D. Labonte, W. Federle, Scaling and biomechanics of surface attachment
9 in climbing animals, Philos Trans R Soc Lond B Biol Sci 370 (1661) (2015)
10 20140027. doi:10.1098/rstb.2014.0027.
- 11 [4] R. D. O’Rorke, T. W. J. Steele, H. K. Taylor, Bioinspired fibrillar adhesives:
12 a review of analytical models and experimental evidence for adhesion en-
13 hancement by surface patterns, J Adhes Sci Technol 30 (4) (2016) 362–391.
14 doi:10.1080/01694243.2015.1101183.
- 15 [5] V. L. Popov, A. É. Filippov, S. N. Gorb, Biological microstructures with
16 high adhesion and friction. numerical approach, Physics-Uspekhi 59 (2016)
17 829–845.
- 18 [6] B. N. J. Persson, On the mechanism of adhesion in biological systems, J
19 Chem Phys 118 (16). doi:10.1063/1.1562192.
- 20 [7] A. Jagota, J. B. Stephen, Mechanics of adhesion through a fibrillar mi-
21 crostructure, Integr Comp Biol 42 (6) (2002) 1140–1145.
- 22 [8] K. Kendall, Thin-film peeling-the elastic term, J Phys D Appl Phys 8 (13)
23 (1975) 1449–1452. doi:10.1088/0022-3727/8/13/005.
- 24 [9] T. Endlein, A. Ji, D. Samuel, N. Yao, Z. Wang, W. J. P. Barnes, W. Federle,
25 M. Kappl, Z. Dai, Sticking like sticky tape: tree frogs use friction forces
26 to enhance attachment on overhanging surfaces, J R Soc Interface 10 (80)
27 (2013) 20120838. doi:10.1098/rsif.2012.0838.

- 1 [10] C. Y. Hui, N. J. Glassmaker, T. Tang, A. Jagota, Design of biomimetic
2 fibrillar interfaces: 2. mechanics of enhanced adhesion, J R Soc Interface
3 1 (1) (2004) 35–48. doi:10.1098/rsif.2004.0005.
- 4 [11] Y. Tian, N. Pesika, H. Zeng, K. Rosenberg, B. Zhao, P. McGuiggan, K. Au-
5 tumn, J. Israelachvili, Adhesion and friction in gecko toe attachment and
6 detachment, Proc Natl Acad Sci U S A 103 (51) (2006) 19320–19325.
7 doi:10.1073/pnas.0608841103.
- 8 [12] A. Pantano, N. M. Pugno, S. N. Gorb, Numerical simulations demonstrate
9 that the double tapering of the spatulae of lizards and insects maximize
10 both detachment resistance and stability, International Journal of Fracture
11 171 (2) (2011) 169–175. doi:10.1007/s10704-011-9596-8.
- 12 [13] R. A. Sauer, M. Holl, A detailed 3d finite element analysis of the peeling
13 behaviour of a gecko spatula, Computer Methods in Biomechanics and
14 Biomedical Engineering 16 (6) (2013) 577–591. doi:10.1080/10255842.
15 2011.628944.
- 16 [14] X. Wu, X. Wang, T. Mei, S. Sun, Mechanical analyses on the digital
17 behaviour of the tokay gecko (*Gekko gekko*) based on a multi-level di-
18 rectional adhesion model, Proceedings of the Royal Society A: Mathe-
19 matical, Physical and Engineering Sciences 471 (2179) (2015) 20150085.
20 doi:10.1098/rspa.2015.0085.
- 21 [15] Y. Kligerman, P. Breitman, M. Varenberg, Biomimetic wall-shaped hier-
22 archical micro-structure: Numerical simulation of sliding inception, Bioin-
23 spiration & Biomimetics 15 (4) (2020) 046011. doi:10.1088/1748-3190/
24 ab8ba3.
- 25 [16] M. J. Grill, C. Meier, W. A. Wall, Investigation of the peeling and pull-
26 off behavior of adhesive elastic fibers via a novel computational beam in-
27 teraction model, The Journal of Adhesion 97 (8) (2021) 730–759. doi:
28 10.1080/00218464.2019.1699795.

- 1 [17] S. Gouravaraju, R. A. Sauer, S. S. Gautam, On the presence of a critical
2 detachment angle in gecko spatula peeling - a numerical investigation using
3 an adhesive friction model, *The Journal of Adhesion* 97 (13) (2021) 1234–
4 1254. doi:10.1080/00218464.2020.1746652.
- 5 [18] A. del Campo, C. Greiner, E. Arzt, Contact shape controls adhesion of
6 bioinspired fibrillar surfaces, *Langmuir* 23 (20) (2007) 10235–10243. doi:
7 10.1021/la7010502.
- 8 [19] M. P. Murphy, B. Aksak, M. Sitti, Adhesion and anisotropic friction en-
9 hancements of angled heterogeneous micro-fiber arrays with spherical and
10 spatula tips, *Journal of Adhesion Science and Technology* 21 (12-13) (2007)
11 1281–1296. doi:10.1163/156856107782328380.
- 12 [20] Y. Mengüç, S. Y. Yang, S. Kim, J. A. Rogers, M. Sitti, Gecko-inspired
13 controllable adhesive structures applied to micromanipulation, *Advanced*
14 *Functional Materials* 22 (6) (2012) 1246–1254. doi:[https://doi.org/10.](https://doi.org/10.1002/adfm.201101783)
15 [1002/adfm.201101783](https://doi.org/10.1002/adfm.201101783).
- 16 [21] S. Chary, J. Tamelier, K. Turner, A microfabricated gecko-inspired con-
17 trollable and reusable dry adhesive, *Smart Materials and Structures* 22 (2)
18 (2013) 025013. doi:10.1088/0964-1726/22/2/025013.
- 19 [22] J.-K. Kim, M. Varenberg, Biomimetic wall-shaped adhesive microstruc-
20 ture for shear-induced attachment: the effects of pulling angle and prelimi-
21 nary displacement, *Journal of The Royal Society Interface* 14 (137) (2017)
22 20170832. doi:10.1098/rsif.2017.0832.
- 23 [23] K. Autumn, Y. A. Liang, S. T. Hsieh, W. Zesch, W. P. Chan, T. W. Kenny,
24 R. Fearing, R. J. Full, Adhesive force of a single gecko foot-hair, *Nature*
25 405 (6787) (2000) 681–685. doi:10.1038/35015073.
- 26 [24] M. G. Langer, J. P. Ruppertsberg, S. Gorb, Adhesion forces measured at
27 the level of a terminal plate of the fly’s seta, *Proceedings of the Royal*

1 Society of London. Series B: Biological Sciences 271 (1554) (2004) 2209–
2 2215. doi:10.1098/rspb.2004.2850.

3 [25] M. Varenberg, N. M. Pugno, S. N. Gorb, Spatulate structures in biolog-
4 ical fibrillar adhesion, *Soft Matter* 6 (2010) 3269–3272. doi:10.1039/
5 C003207G.

6 [26] W. Federle, Why are so many adhesive pads hairy?, *J Exp Biol* 209 (Pt
7 14) (2006) 2611–21. doi:10.1242/jeb.02323.

8 [27] J. M. Bullock, W. Federle, Division of labour and sex differences be-
9 tween fibrillar, tarsal adhesive pads in beetles: effective elastic modulus
10 and attachment performance, *J Exp Biol* 212 (Pt 12) (2009) 1876–1888.
11 doi:10.1242/jeb.030551.

12 [28] G. Carbone, E. Pierro, S. N. Gorb, Origin of the superior adhesive perfor-
13 mance of mushroom-shaped microstructured surfaces, *Soft Matter* 7 (12)
14 (2011) 5545–5552. doi:10.1039/C0SM01482F.

15 [29] L. Heepe, G. Carbone, E. Pierro, A. E. Kovalev, S. N. Gorb, Adhesion tilt-
16 tolerance in bio-inspired mushroom-shaped adhesive microstructure, *Ap-
17 plied Physics Letters* 104 (1) (2014) 011906. doi:10.1063/1.4860991.

18 [30] D. Paretkar, M. Kamperman, D. Martina, J. Zhao, C. Creton, A. Lindner,
19 A. Jagota, R. McMeeking, E. Arzt, Preload-responsive adhesion: effects
20 of aspect ratio, tip shape and alignment, *J R Soc Interface* 10 (83) (2013)
21 20130171. doi:10.1098/rsif.2013.0171.

22 [31] D.-M. Drotlef, P. Blümner, A. del Campo, Magnetically actuated patterns
23 for bioinspired reversible adhesion (dry and wet), *Adv Mater* 26 (5) (2014)
24 775–779. doi:10.1002/adma.201303087.

25 [32] E. Kizilkan, J. Strueben, A. Staubitz, S. N. Gorb, Bioinspired photocontrol-
26 lable microstructured transport device, *Sci Robot* 2 (2) (2017) eaak9454.
27 doi:10.1126/scirobotics.aak9454.

- 1 [33] J. Cui, D.-M. Drotlef, I. Larraza, J. P. Fernández-Blázquez, L. F. Boesel,
2 C. Ohm, M. Mezger, R. Zentel, A. del Campo, Bioinspired actuated ad-
3 hesive patterns of liquid crystalline elastomers, *Adv Mater* 24 (34) (2012)
4 4601–4604. doi:<https://doi.org/10.1002/adma.201200895>.
- 5 [34] M. Schargott, V. L. Popov, S. Gorb, Spring model of biological attachment
6 pads, *J Theor Biol* 243 (1) (2006) 48–53. doi:[https://doi.org/10.1016/](https://doi.org/10.1016/j.jtbi.2006.05.023)
7 [j.jtbi.2006.05.023](https://doi.org/10.1016/j.jtbi.2006.05.023).
- 8 [35] M. Bacca, J. A. Booth, K. L. Turner, R. M. McMeeking, Load sharing in
9 bioinspired fibrillar adhesives with backing layer interactions and interfacial
10 misalignment, *J Mech Phys Solids* 96 (2016) 428–444. doi:[https://doi.](https://doi.org/10.1016/j.jmps.2016.04.008)
11 [org/10.1016/j.jmps.2016.04.008](https://doi.org/10.1016/j.jmps.2016.04.008).
- 12 [36] J. M. Bullock, W. Federle, Beetle adhesive hairs differ in stiffness and
13 stickiness: in vivo adhesion measurements on individual setae, *Naturwis-*
14 *senschaften* 98 (5) (2011) 381–387. doi:[10.1007/s00114-011-0781-4](https://doi.org/10.1007/s00114-011-0781-4).
- 15 [37] R. Hensel, J. Thiemecke, J. A. Booth, Preventing catastrophic failure of
16 microfibrillar adhesives in compliant systems based on statistical analysis of
17 adhesive strength, *ACS Appl Mater Interfaces* 13 (16) (2021) 19422–19429.
18 doi:[10.1021/acsami.1c00978](https://doi.org/10.1021/acsami.1c00978).
- 19 [38] M. Kamperman, E. Kroner, A. del Campo, R. M. McMeeking, E. Arzt,
20 Functional adhesive surfaces with “gecko” effect: The concept of contact
21 splitting, *Advanced Engineering Materials* 12 (5) (2010) 335–348. doi:
22 <https://doi.org/10.1002/adem.201000104>.
- 23 [39] J. A. Booth, M. Bacca, R. M. McMeeking, K. L. Foster, Benefit of backing-
24 layer compliance in fibrillar adhesive patches-resistance to peel propagation
25 in the presence of interfacial misalignment, *Adv Mater Interfaces* 5 (15)
26 (2018) 1800272. doi:<https://doi.org/10.1002/admi.201800272>.
- 27 [40] S. M. Gernay, S. Labousse, P. Lambert, P. Compere, T. Gilet, Multi-scale

1 tarsal adhesion kinematics of freely-walking dock beetles, J R Soc Interface
2 14 (136) (2017) 20170493. doi:10.1098/rsif.2017.0493.

3 [41] S. Niederegger, S. Gorb, Tarsal movements in flies during leg attachment
4 and detachment on a smooth substrate, Journal of Insect Physiology 49 (6)
5 (2003) 611–620. doi:10.1016/s0022-1910(03)00048-9.

6 [42] O. H. Kang, S. H. Lee, J. H. Yun, H. Yi, M. K. Kwak, S. R. Lee, Adhesion
7 tunable bio-inspired dry adhesives by twisting, International Journal of
8 Precision Engineering and Manufacturing 18 (10) (2017) 1433–1437. doi:
9 10.1007/s12541-017-0171-8.

10 [43] H. Peisker, J. Michels, S. N. Gorb, Evidence for a material gradient in the
11 adhesive tarsal setae of the ladybird beetle *Coccinella septempunctata*, Nat
12 Commun 4 (2013) 1661. doi:10.1038/ncomms2576.

13 [44] T. Endlein, W. Federle, To stick and not getting stuck — detachment
14 control in ants, Comparative Biochemistry and Physiology Part A: Molec-
15 ular & Integrative Physiology 146 (4, Supplement) (2007) S121–S122, ab-
16 stracts of the Annual Main Meeting of the Society for Experimental Bi-
17 ology, Glasgow, Scotland, 31st March - 4th April, 2007. doi:https:
18 //doi.org/10.1016/j.cbpa.2007.01.222.